https://doi.org/10.5194/angeo-2021-28
Preprint. Discussion started: 10 June 2021

Annales Geophysicae Discussions
Open Access

What caused the frequent and widespread occurrences of noctilucent clouds at middle latitudes in 2020?

Peter Dalin[1,2*], Hidehiko Suzuki[3], Nikolay Pertsev[4], Vladimir Perminov[4], Nikita Shevchuk[5], Egor Tsimerinov[6], Mark Zalcik[7], Jay Brausch[7], Tom McEwan[8], Iain McEachran[8], Martin Connors[9], Ian Schofield[9], Audrius Dubietis[10], Kazimieras Černis[11], Alexander Zadorozhny[12], Andrey Solodovnik[13] , Daria Lifatova[14], Jesper Grønne[15], Ole Hansen[15], Holger Andersen[15], Dmitry Melnikov[16], Alexander Manevich[16], Nikolay Gusev[17], Vitaly Romejko[†17]

† deceased

[1]Swedish Institute of Space Physics, Box 812, SE-981 28 Kiruna, Sweden
[2]Space Research Institute, RAS, Profsouznaya st. 84/32, Moscow 117997, Russia
[3]Meiji University, Kawasaki, Kanagawa, Japan
[4]A. M. Obukhov Institute of Atmospheric Physics, RAS, Pyzhevskiy per., 3, Moscow 119017, Russia
[5]Saint Petersburg State University, Department of Atmospheric Physics, Ul`yanovskaya str., 1, Petergof, Saint Petersburg, 198504
[6]Meteoweb.ru, Moscow, Russia
[7]1005-11230 St. Albert Trail, Edmonton, Alberta, T5M 3P2, Canada
[8]NLC NET, 14 Kersland Road, Glengarnock, Ayrshire, KA14 3BA Scotland, UK
[9]Athabasca University Geophysical Observatory, Athabasca, Alberta, Canada T9S 3A3
[10]Laser Research Center, Vilnius University, Sauletekio Ave. 10, LT-10223, Vilnius, Lithuania
[11]Institute of Theoretical Physics and Astronomy, Vilnius University, Sauletekio Ave. 3, LT-10257, Vilnius, Lithuania
[12]Novosibirsk State University, Pirogova st. 2, Novosibirsk 630090, Russia
[13]M. Kozybaev North Kazakhstan State University, Petropavlovsk, Kazakhstan
[14]The Faculty of Physics, M. V. Lomonosov Moscow State University, 1-2, Leninskie Gory, Moscow, 119991
[15]The Danish Association for NLC Research, Spurvevænget 14, Ejby, Lille Skensved, DK-2623, Denmark
[16]Institute of Volcanology and Seismology, RAS, 9 Piip Boulevard, Petropavlovsk-Kamchatsky, 683006, Russia
[17]The Moscow Association for NLC Research, Kosygina st. 17, 119334 Moscow, Russia

*Corresponding author: Peter Dalin, Tel: +46-980-79023, E-mail: pdalin@irf.se

https://doi.org/10.5194/angeo-2021-28
Preprint. Discussion started: 10 June 2021

Annales Geophysicae Discussions

Highlights:

1. The 2020 summer season revealed frequent NLCs in the NH at middle latitudes
2. A moderate decrease in summer mesopause temperature was observed between 2016-2020
3. H_2O mixing ratio in the upper mesosphere increased in summer 2020 compared to 2017
4. The 2020 H_2O maximum can be explained by a maximum in volcanic activity in 2015

Abstract

The 2020 summer season has revealed frequent occurrences of noctilucent clouds (NLCs) around the Northern hemisphere at middle latitudes (45-55°N), with the lowest latitude at which NLCs were seen being 34.1°N. In order to investigate a reason for this NLC extraordinary summer season, we have analyzed long-term Aura/MLS satellite data for all available summer periods from 2005 to 2020. Both Aura/MLS summer temperature and water vapor in the upper mesosphere and the mesopause region, between 74 and 89 km altitude, have been considered. We have found that there has been a moderate decrease in the upper mesosphere temperature between 2016 and 2020 and no dramatic changes have been observed in temperature in the summer of 2020 at the middle latitude mesopause. At the same time, water vapor concentration has significantly increased (by about 12-15%) in the zonal mean H_2O value in the 2020 summer compared to 2017, meaning that the summer mesopause at middle latitudes has become more wet. At the same time, no increase in water vapor has been detected at the high latitude high altitude mesopause. A combination of lower mesopause temperature and water vapor concentration maximum at middle latitudes is the main reason for frequent and widespread occurrences of NLCs seen around the globe at middle latitudes in the summer of 2020. The 24th solar cycle minimum cannot explain the H_2O maximum in 2020 since the correlation between Lyman-α flux and the amount of water vapor is low. The increase in volcanic activity from 2013 to 2015 (and its recent maximum occurred in 2015) explains the increased amount of water vapor in the upper mesosphere for the past years and its maximum in 2020 due to volcanic water vapor being injected into the atmosphere and transported into the upper mesosphere. The 5-year delay between volcanic activity and water vapor maximum is well explained by a general meridional-vertical atmospheric circulation.

Keywords: noctilucent clouds, upper mesosphere, volcanic activity, solar activity

https://doi.org/10.5194/angeo-2021-28
Preprint. Discussion started: 10 June 2021

Annales Geophysicae
Discussions
Open Access

1. Introduction

The highest clouds in the Earth's atmosphere are noctilucent clouds (NLCs) formed around the mesopause region at 80–90 km altitudes. The clouds are a beautiful nighttime optical phenomenon occurring during the summer months at middle, subpolar and high latitudes. NLCs consist of water ice particles of 30–100 nm in radius that scatter sunlight and thus NLCs are readily seen within the arc of twilight from middle of May until end of August (Gadsden and Schröder, 1989).

Satellite observations have discovered polar mesospheric clouds (PMCs) covering almost the entire polar mesopause region poleward of ±70° latitude during summertime (Donahue et al., 1972; Thomas, 1984; Russell III et al., 2009). Sometimes, some areas or "patches" of PMCs (similar to icebergs separating from a continental ice sheet) extend to mid-latitudes and become visible from the Earth's surface as NLCs. A number of NLC observations were from as far south as at latitudes of 39-42°N (Taylor et al., 2002; Wickwar et al., 2002; Herron et al., 2007; Nielsen et al., 2011). A great enhancement of NLCs was noticed in July 2009 at middle latitudes: NLCs were seen in many countries in Europe and as far south as Palmela (Portugal) and Colorado (USA) at ~39°N (Nielsen et al., 2011). A single NLC observation was observed from Hokkaido, Japan (43.2–44.4°N) in June 2015 (Suzuki et al., 2016). Occasional NLC observations at mid-latitudes, limited in space and time, have not allowed us to resolve the main source of NLC formation and variability at mid-latitudes so far. Hultgren et al. (2011) have demonstrated that NLC enhancements observed in July 2009 were produced locally due to cold mesopause temperatures provided by lower average mesopause temperature (compared to previous years), diurnal tides and large-scale planetary waves, with the NLC/PMC transport from polar to middle latitudes being questionable because of a short life-time of visible (bright) NLCs. However, Nielsen et al. (2011), studying the same NLC increase in July 2009, have found those bright NLCs occurred due to a combination of additional wave cooling (the 2-, 5- and 16-day planetary waves) and advection of NLCs from higher to middle latitudes. Gerding et al. (2013a,b) have analyzed long-term midlatitude lidar measurements of NLCs at Kühlungsborn, Germany (54°N).They have also found an NLC maximum in 2009 with a rate of 19%.

In the present study, we report on the latest outbreak of NLC activity, which happened in the summer of 2020 at middle northern latitudes. We focus our investigation on NLC sightings seen at latitudes below 50°N by analyzing various NLC databases. An analysis of Aura satellite data (temperature and water vapor) for summers 2005–2020 is applied to different latitudes and altitudes in the upper mesosphere and the mesopause region in order to establish a reason for the

https://doi.org/10.5194/angeo-2021-28
Preprint. Discussion started: 10 June 2021

2020 extraordinary NLC season. Solar and volcanic activities are considered to investigate their roles in the budget of water vapor in the upper mesosphere.

2. Data Source

Various ground-based NLC observations around the world have been considered in order to compare the latest outbreak of NLCs happening in the summer of 2020. We have analyzed the North America (Canada and USA, CAN AM, https://www.researchgate.net/profile/M-Zalcik/research) NLC database for the period of 2005–2020, the West European NLC database for 2005–2020 (http://ed-co.net/nlcnet/pos15-may) as well as the Russian NLC database for 2009–2020 (http://meteoweb.ru/astro/nlc/reports.php). Most of the NLC observations in these countries have been conducted by professional NLC observers for many years, and most NLC reported are accompanied by photographic registrations (the reader can find details of NLC observations on these web resources). Note that part of these NLC observations include monitoring by high quality automated digital cameras, taking images of the night sky every minute during entire summer season, which are situated through the entire Northern Hemisphere (Dalin et al., 2008; Dubietis et al., 2011).

The Microwave Limb Sounder (MLS) radiometer onboard NASA Aura satellite is used as a source of temperature and water vapor data (Waters et al., 2006). On 15 July 2004, Aura was launched into a near-polar (98° inclination), sun-synchronous orbit 705 km above the Earth, with ascending and descending equator-crossing times at 13:45 and 01:45 local time, respectively. The orbital period is about 100 minutes. Since the Aura orbit is nearly fixed in solar local time, Aura makes measurements for a given point in the atmosphere twice a day (ascending and descending transversals); the number of orbits per day is around 14.6. The temperature and water vapor data of the MLS instrument from 25 May to 13 August from 2005 to 2020 are used in this study. The description on the MLS temperature product and its validation can be found in Froidevaux et al. (2006) and Schwartz et al. (2008). The validation of water vapor data is described in detail by Read et al. (2007) and Lambert et al. (2007). The Aura/MLS temperature and water vapor of ver.4.23 and level 2 data quality have been obtained from the NASA public web-site: https://acdisc.gesdisc.eosdis.nasa.gov/data/Aura_MLS_Level2/

3. Method of Analysis

The Aura/MLS instrument measures temperature and water vapor on the day and night side of the Earth (twice a day at each longitude). The temperature in the upper mesosphere experiences large diurnal variations due to solar tides of about 5–15 K between 60° and 50°N (Hultgren et al.,

https://doi.org/10.5194/angeo-2021-28
Preprint. Discussion started: 10 June 2021

Annales Geophysicae Discussions Open Access EGU

2011). That is why we analyze nighttime temperature corresponding to a colder phase of solar tides (Stevens et al., 2017) and nighttime water vapor measurements to use those most likely related to the formation and existence of NLCs at middle latitudes. Nighttime values of neutral temperature and water vapor have been averaged over the following latitudes bands: 45–50°, 50–55° and 55–60°N. Zonal mean temperature and water vapor values have been considered for the following four pressure levels: 0.0215 hPa (about 74 km), 0.01 hPa (about 79 km), 0.0046 hPa (about 84 km), and 0.0022 hPa (about 89 km).

Since temperature variations exhibit a decrease/increase in the first/second half of a summer, an inverse Gaussian fit in the least-square sense has been estimated to temperature variations for each summer season of 2005–2020, with a summer season being considered between 25 May and 13 August. Water vapor behaves, generally, in opposite way, that is there is an increase/decrease in the first/second half of a summer season. That is why a Gaussian fit has been estimated in the least-square sense to H_2O volume mixing ratio variations for each analyzed summer season. The volume mixing ratio of H_2O defines the fractional concentration of water vapor as the number of H_2O molecules per million air molecules and expressed in units of parts per million by volume (ppmv). An example of temperature and water vapor data at the latitude band of 45-50°N at 0.0046 hPa for the 2009 summer is illustrated in Fig. 1. As a result, we further analyze three different statistical parameters of temperature and water vapor measurements:

a) mean of zonal mean nighttime temperatures and water vapor for a summer season (25 May – 13 August);

b) minimum / maximum value of zonal mean nighttime temperature / water vapor data, respectively, for a summer season;

c) minimum / maximum value of a Gaussian fit to temperature / water vapor data, respectively, for a summer season.

https://doi.org/10.5194/angeo-2021-28
Preprint. Discussion started: 10 June 2021

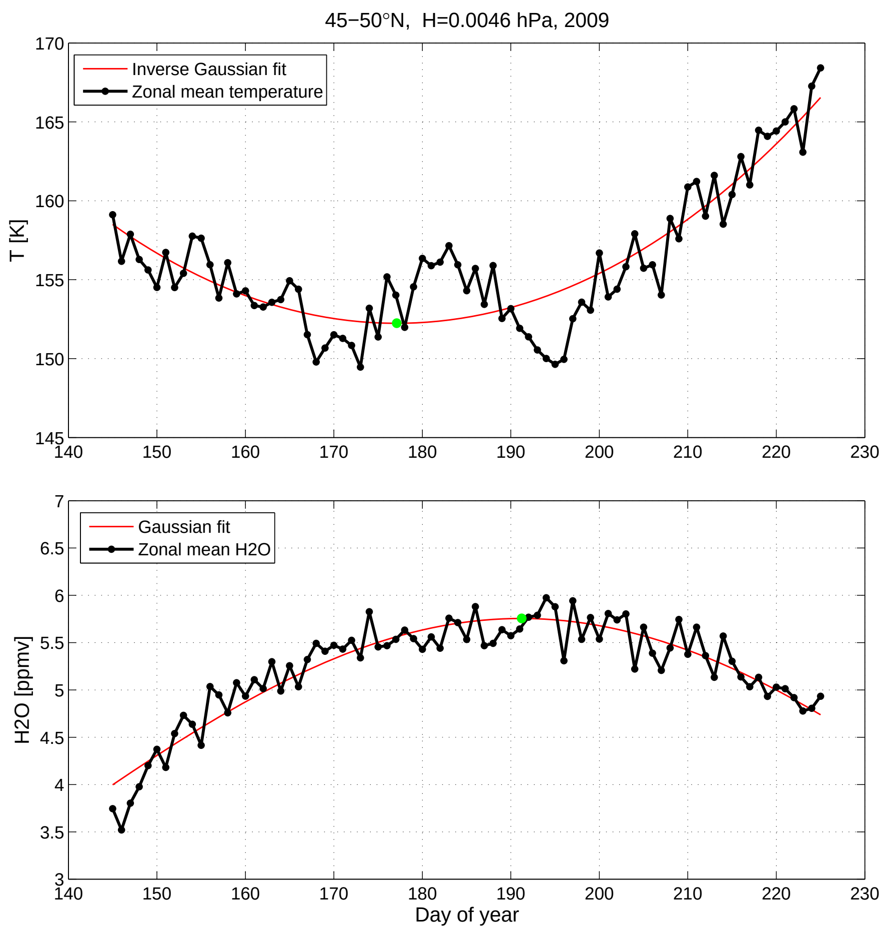

Figure 1. An example of Aura/MLS data shown at the latitude band of 45-50°N at 0.0046 hPa (about 84 km) during the summer time between 25 May and 13 August 2009. (Upper panel) Zonal mean nighttime temperatures (the black line with dots), the red curve represents an inverse Gaussian fit to the data, the green dot shows the minimum of a Gaussian fit. (Lower panel) Zonal mean nighttime H_2O mixing ratio values (the black line with dots), the red curve shows a Gaussian fit to the data, the green dot marks the maximum of a Gaussian fit.

4. Results

4.1. Results on noctilucent clouds activity

The outstanding 2020 NLC season started with early observations of NLCs on 22/23, 23/24 and 24/25 May seen from many sites in Russia. On 29/30 May, NLCs were registered at Ft. Chipewyan, Stony Rapids and Key Lake in Canada (57-59°N). At middle latitudes (~47°N), NLC were first seen from Switzerland on 30/31 May (see https://www.foto-

https://doi.org/10.5194/angeo-2021-28
Preprint. Discussion started: 10 June 2021

webcam.eu/webcam/pizol/2020/05/31/0340). Then NLCs were observed nearly every night at the beginning of June 2020 from North America (as south as Logan, Utah, 41.7°N).

A remarkable feature of the 2020 summer season is that NLC displays were seen from Hokkaido (Japan) at latitudes between 43° and 44°N in the middle of June (12, 13, 14) and on 18 July. Note that before the 2020 summer, NLCs were observed from Hokkaido only once, on 21 June 2015, in spite of the fact that NLC observations are conducted every summer from 2010 with multiple automated cameras located at Hokkaido (Suzuki et al., 2016). Thus, NLC events seen four times from Hokkaido are an extraordinary feature of the 2020 summer season. An example of the NLC display seen from Hokkaido on 18/19 June 2020 is shown in Fig. 2.

Note that at higher latitudes of 55-60°N, NLC activity behaved differently from site to site. For example, maxima in the NLC occurrence number have been observed in Edmonton (Alberta, Canada, ~53°N) with 28 NLC cases in 2020, and in Lithuania (54-55°N) with 42 NLC cases in 2020 in the past 30 years, whereas NLC activity had no maximum in 2020 as seen from the Moscow region (55-56°N) in the past 60 years, taking into account tropospheric weather conditions. The reason for this will be addressed in the Discussion. At the same time, a maximum in NLC sightings (73 cases) has been registered in North America as observed from many sites, meaning that NLCs were seen on almost every night in the 2020 summer across North America. The farthest-south NLC display was evident on 3/4 July from Joshua Tree, California, USA at 34.1°N. The 2020 NLC season lasted for a long time until 19/20 August as evident from an observation on that date in Cape Dorset in Canada (64.2°N). There was also an unusually late NLC sighting on 13/14 August as seen from the Moscow Region (56°N).

https://doi.org/10.5194/angeo-2021-28
Preprint. Discussion started: 10 June 2021

Figure 2. An example image of noctilucent clouds as seen from Hokkaido, Japan (44.3°N, 142.2°E) on the night of 17/18 July 2020. Comet NEOWISE is clearly seen in the image. The NLC photograph taken from Hokkaido has been provided by a staff of Nayoro astronomy observatory, Mr. Fumitake Watanabe.

We have carefully analyzed three NLC databases: North America (Canada and USA), Western Europe and Russia for the period of 2005–2020. For consistency purposes, the number of NLC sightings observed at latitudes below 50°N has been counted, which is shown in Fig. 3. One can clearly see that all three databases demonstrate the maximum of NLC sightings in 2020, with significantly increased NLC numbers by North America and Russian observations (the black and blue lines).

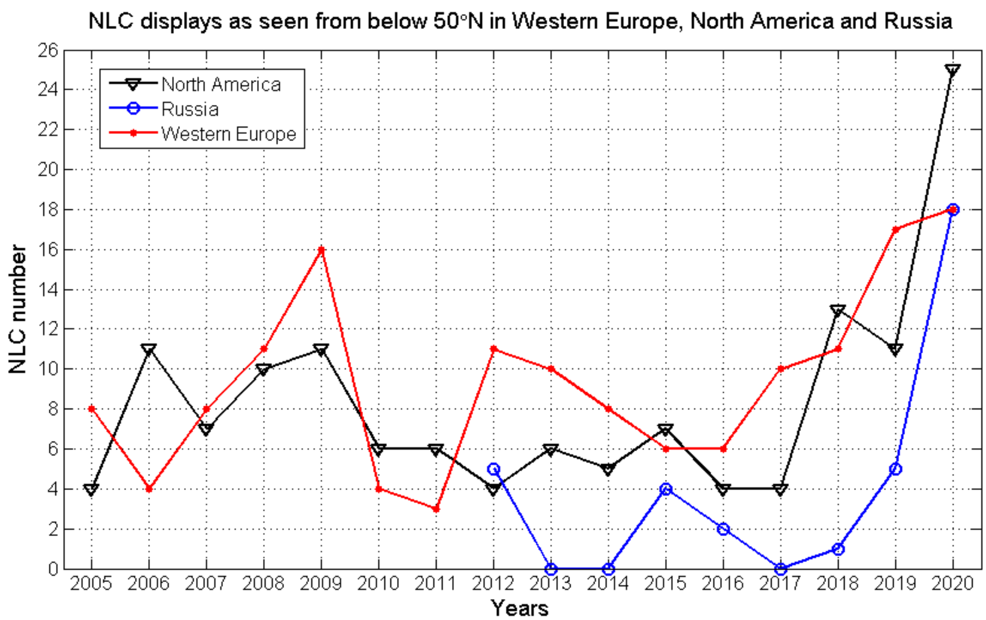

Figure 3. The number of displays of noctilucent clouds as observed from latitudes below 50°N as a function of time. The black line with triangles shows NLC displays as observed in North America (Canada and USA observations), the blue line with open circles illustrates NLC sightings as observed from Russia, the red line with dots is NLC events as seen from Western Europe.

4.2. Results on temperature and water vapor analysis

Figures 4 and 5 illustrate three different statistical parameters of Aura/MLS temperature time series for 2005–2020 as described in section 3. Figure 4 demonstrates a general decrease in

https://doi.org/10.5194/angeo-2021-28
Preprint. Discussion started: 10 June 2021

Annales Geophysicae
Discussions
Open Access

temperature starting from 2016/2017 until 2020. One can also see a temperature minimum in 2009 (Fig. 4b,d,f) as previously discussed in the literature (Hultgren et al., 2011; Nielsen et al., 2011). The most significant decrease in temperature has been observed at the latitude bands of 50-55° and 55-60°N at the lowest considered pressure level of 0.0215 hPa (Fig. 4c,e), with the lowest temperature values observed in all three statistical parameters in the 2020 summer. At the bottom of the mesopause region (0.01 hPa, about 79 km), the 2020 temperature drop is rather moderate, having about the same values as ones observed in 2009.

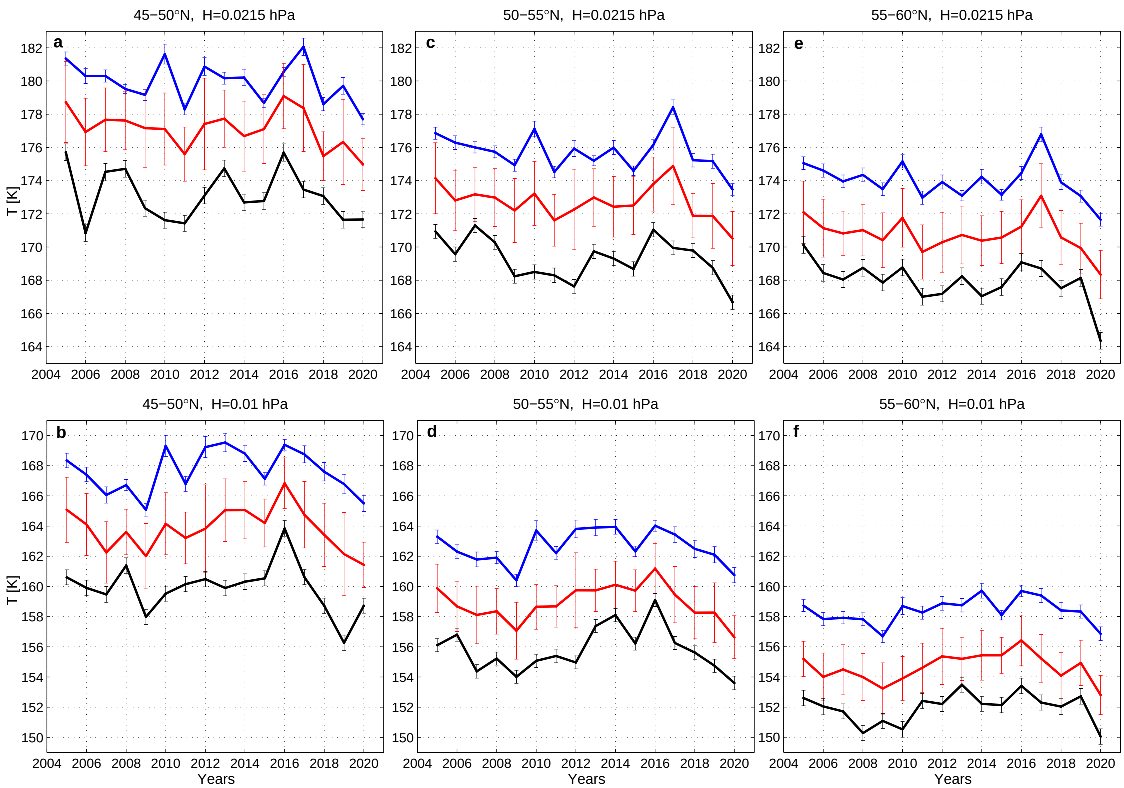

Figure 4. Aura/MLS temperature time series for summer periods of 2005–2020 at different latitude bands (45-50; 50-55; 55-60°N) and pressure levels of 0.0215 hPa (about 74 km) and 0.01 hPa (about 79 km). The black line indicates a minimum value of the zonal mean nighttime temperature for a summer season (between 25 May and 13 August), the red line is a minimum value of an inverse Gaussian fit, the blue line shows the mean of the zonal mean nighttime temperature for a summer period. Error bars indicate one standard deviation for each point.

https://doi.org/10.5194/angeo-2021-28
Preprint. Discussion started: 10 June 2021

Figure 5 shows a complicated temperature behavior at 0.0046 hPa (about 84 km) and 0.0022 hPa (about 89 km) pressure levels for summers 2005–2020. At 45-50° and 50-55°N latitude bands at 0.0046 hPa (Fig. 5a,c,e), a general temperature decrease has been observed since 2014-2016; however the temperature in the summer 2020 (different statistical parameters) was not the lowest one for the considered time interval of 2005–2020. The lowest temperatures were observed in the summer of 2008, 2009, 2010 and 2019, depending on latitude band and temperature statistical parameters. At the pressure level of 0.0022 hPa (Fig. 5b,d,f), the summer temperatures have been increasing since 2017 and no dramatic changes have been observed in the 2020 summer temperature at this altitude, which is the top of the summer mesopause region.

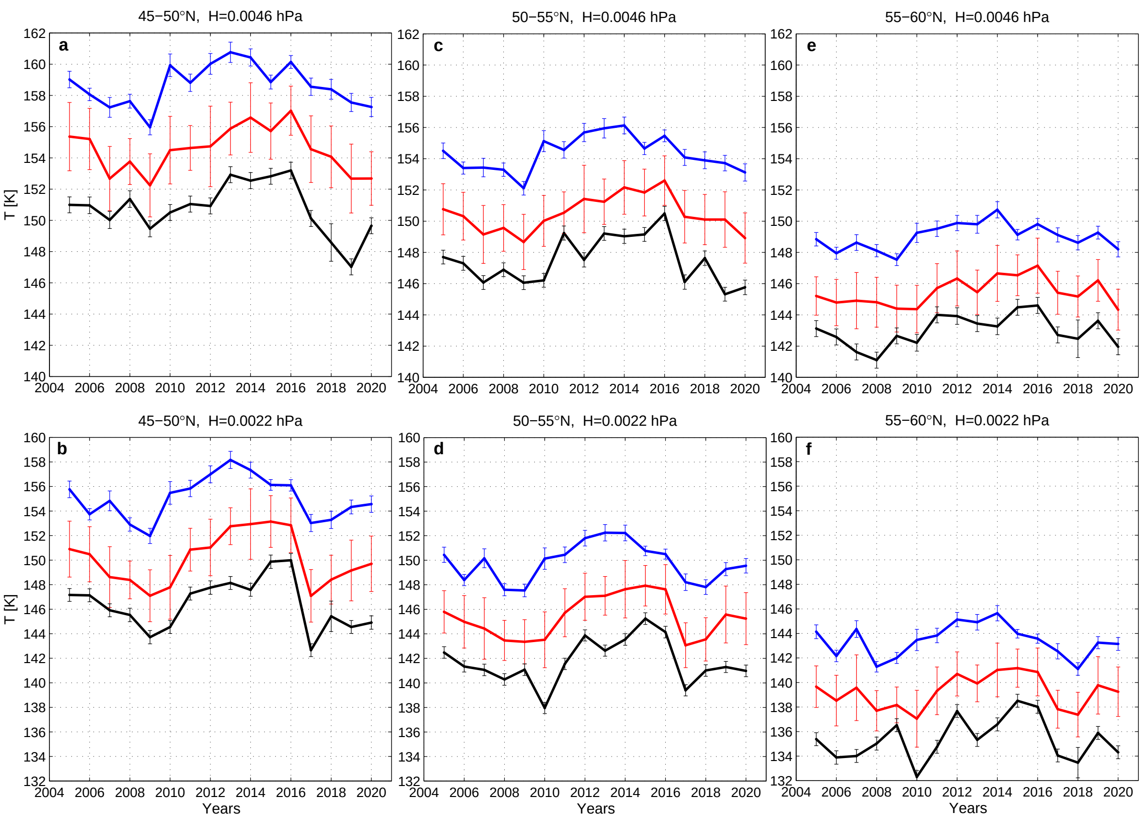

Figure 5. Aura/MLS temperature time series for summer periods of 2005–2020 at different latitude bands (45-50; 50-55; 55-60°N) and pressure levels of 0.0046 and 0.0022 hPa. The black line indicates a minimum value of the zonal mean nighttime temperature for a summer season (between 25 May and 13 August), the red line is a minimum value of an inverse Gaussian fit, the blue line shows the mean of the zonal mean nighttime temperature for a summer period. Error bars indicate one standard deviation for each point.

https://doi.org/10.5194/angeo-2021-28
Preprint. Discussion started: 10 June 2021

Figures 6 and 7 illustrate three different statistical parameters of Aura/MLS water vapor time series for 2005–2020 as described in section 3. Figure 6 demonstrates a strong increase in the water vapor concentration between 2017 and 2020 at all considered latitude bands (45-50; 50-55; 55-60°N) at two pressure levels of 0.0215 and 0.01 hPa. All statistical parameters show the highest values in the H_2O concentration in the last 16 years occurring in the summer of 2020. Starting from the summer 2017, the H_2O mixing ratio has increased by about 12-15% in the zonal mean value, depending on a latitude band and altitude, meaning that the upper mesosphere at these latitudes and altitudes has become more wet.

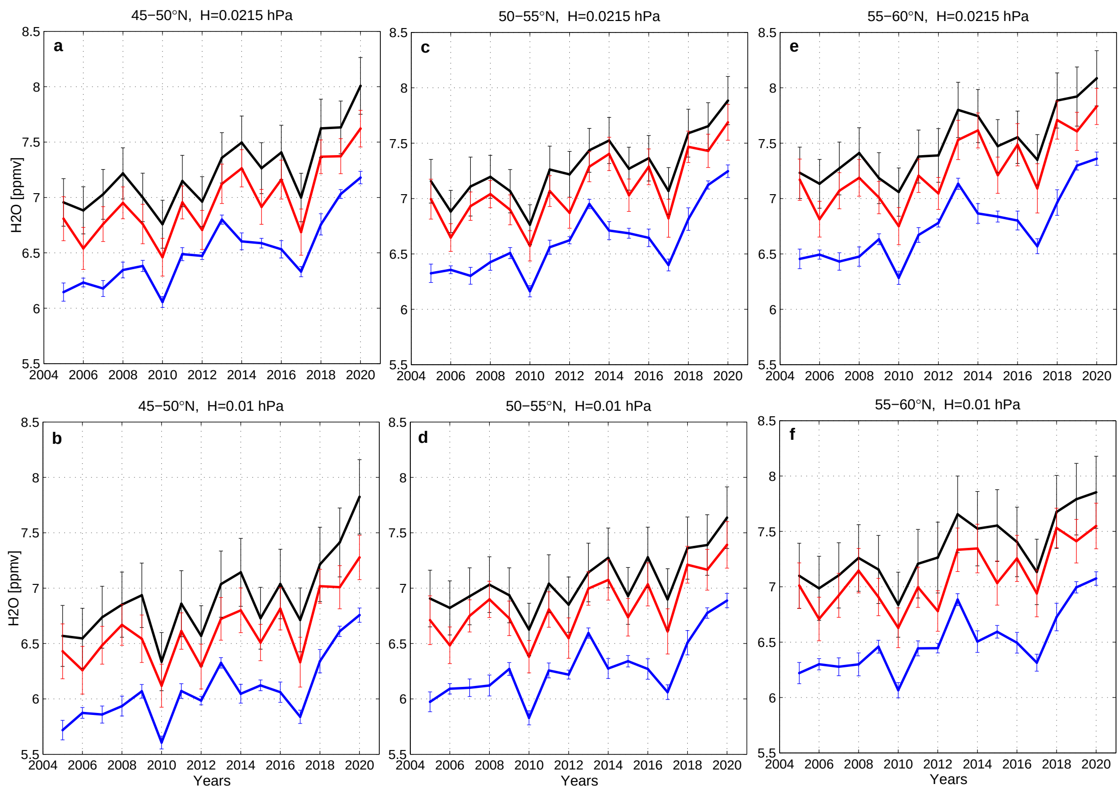

Figure 6. Aura/MLS water vapor mixing ratio [ppmv] time series for summer periods of 2005–2020 at different latitude bands (45-50; 50-55; 55-60°N) and pressure levels of 0.0215 hPa (about 74 km) and 0.01 hPa (about 79 km). The black line indicates a maximum value of the nighttime H_2O zonal mean for a summer season between 25 May and 13 August, the red line is a maximum value of a Gaussian fit, the blue line shows the mean of the nighttime H_2O zonal mean for a summer period. Error bars indicate one standard deviation for each point.

https://doi.org/10.5194/angeo-2021-28
Preprint. Discussion started: 10 June 2021

Annales Geophysicae
Discussions
Open Access
EGU

Figures 7a and 7c illustrate that the maximum in the water vapor concentration has occurred in the 2020 summer at the latitude band of 45-50°N and might be at 50-55°N at the pressure level of 0.0046 hPa. However, at 55-60°N, the H_2O maximum occurred in 2018-2019, depending on the statistical parameters (Fig. 7e). At the same time, there was no H_2O increase in 2020 at the higher level of 0.0022 hPa at all considered latitudes (Fig. 7b,d,f); here the highest H_2O maxima in 16 years were observed in 2018-2019. In general, no dramatic changes in water vapor concentration have been observed at pressure levels of 0.0046 and 0.0022 hPa for the period of 2005–2020.

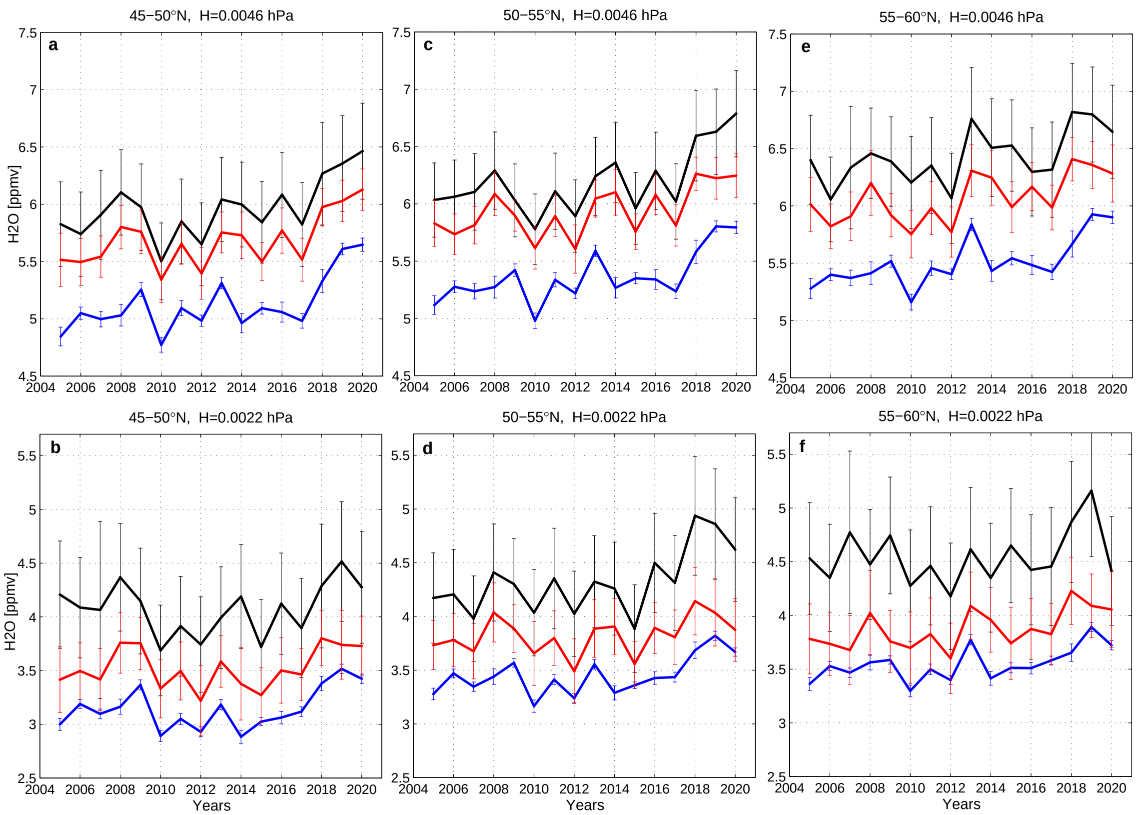

Figure 7. Aura/MLS water vapor mixing ratio [ppmv] time series for summer periods of 2005–2020 at different latitude bands (45-50; 50-55; 55-60°N) and pressure levels of 0.0046 hPa (about 84 km) and 0.0022 hPa (about 89 km). The black line indicates a maximum value of the nighttime H_2O zonal mean for a summer season between 25 May and 13 August, the red line is a maximum value of a Gaussian fit, the blue line shows the mean of the nighttime H_2O zonal mean for a summer period. Error bars indicate one standard deviation for each point.

4.3. Results on the relationship between solar activity and the water vapor concentration maximum in 2020.

https://doi.org/10.5194/angeo-2021-28
Preprint. Discussion started: 10 June 2021

Annales Geophysicae Discussions
Open Access

The recently past 24th solar activity cycle has demonstrated the lowest solar activity in the last 60 years as illustrated in Fig. 8, which shows summer mean solar Lyman alpha flux data obtained from the LASP Interactive Solar Irradiance Datacenter (LISIRD) at http://lasp.colorado.edu/lisird. In the present analysis, we use time series of the Lyman α flux at 121.6 nm as a proxy for solar activity.

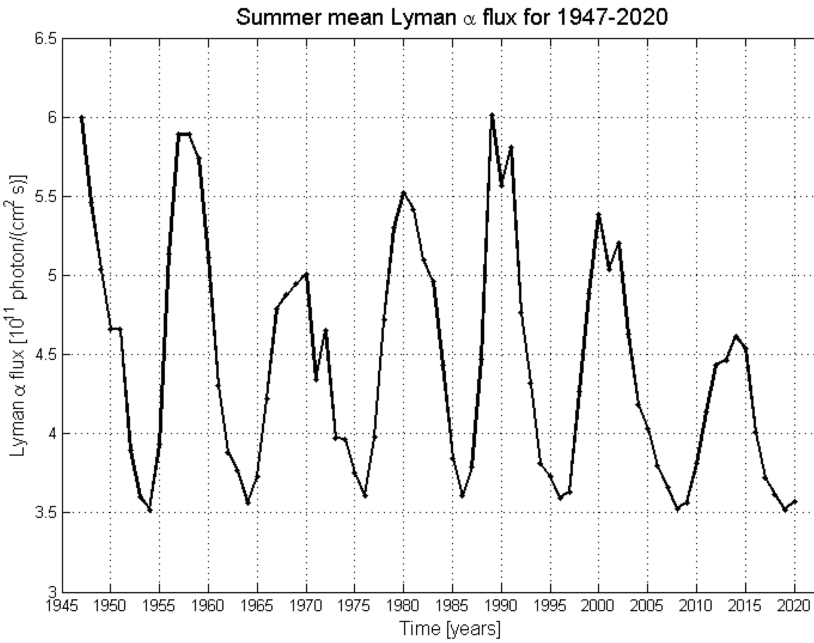

Figure 8. Summer mean values of solar Lyman-α flux for the period of 1947–2020.

It is well-known that Lyman alpha radiation photodissociates water molecules hence decreasing the amount of water vapor in the upper mesosphere and the mesopause region (Brasseur and Solomon, 1986). From this point of view, one can anticipate an anticorrelation behavior between solar Lyman-α flux and amount of water vapor in the mesopause region. Since there was the lowest solar activity in the last 60 years occurred in the summers of 2019 and 2020, one can expect highest values of water vapor concentration in the summer mesopause in 2019 and 2020. We can check this hypothesis by applying the relationship between water vapor measurements and solar activity in a form of the multiple regression analysis (MRA):

$$H2O = C_{01} + C_{11} \cdot (t - 2005) + C_{21} \cdot F_{Lya}(t - t_{lag1}) \qquad (1)$$

https://doi.org/10.5194/angeo-2021-28
Preprint. Discussion started: 10 June 2021

Annales Geophysicae Discussions

where *H2O* is the summer mean water vapour mixing ratio per each year, F_{Lya} is the Lyman α flux averaged over each summer season (June-July), *t* is the time, C_{01} is the regression constant; C_{11} is the regression coefficients characterizing the linear long-term trend (*H2O*/yr), C_{21} is the solar activity term (*H2O*/ per solar Lyman-α flux units, SFU, 1 SFU is 10^{11} photons $s^{-1}cm^{-2}$), t_{lag1} is the phase time lag between water vapor and solar activity. A similar MRA technique has been frequently utilized in geophysical data analysis (Dalin et al., 2020; DeLand and Thomas, 2019; Dubietis et al., 2010; Kirkwood et al., 2008; Pertsev et al., 2014).

Figure 9 demonstrates the relationship between water vapour and solar activity for 2005–2020. Figure 9a shows a cross-correlation coefficient as a function of time lag, which is very low varying between 0 and –0.2. Figure 9b shows the maximum H_2O value of a Gaussian fit estimated at middle latitudes 50-55°N and at pressure level of 0.01 hPa (see the red line in Fig. 6d) as well as the model regression curve (the black line) as calculated using equation 1. We choose a time lag (t_{lag1}) equal to zero years for the $C_{21} \cdot F_{Lya}$ term as calculated from the cross-correlation analysis between water vapor measurements and Lyman-α time series for 2005-2020. The choice of solar time lag does not influence the obtained results since the correlation between Lyman-α flux and water vapor is very low. After the subtraction of the solar term from water vapor measurements using equation 1, we arrive at H_2O residuals shown in Fig. 9c.

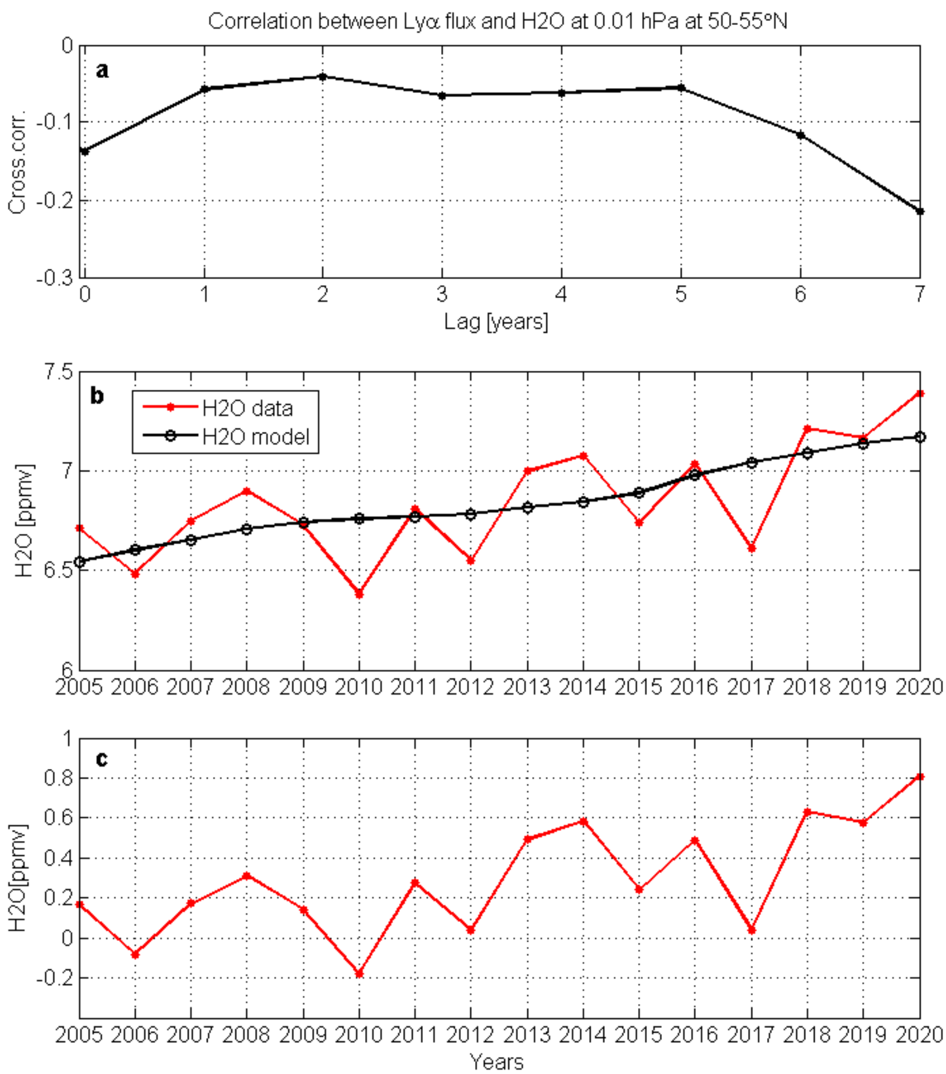

Figure 9. Relationship between water vapor and solar activity for 2005–2020. Solar activity is represented by Lyman-α flux measurements. (a) cross-correlation coefficient as a function of time lag. (b) the red line shows the maximum value of H_2O mixing ratio of a Gaussian fit estimated at middle latitudes 50-55°N at 0.01 hPa (the red line in Fig. 6d), the black line is the model regression curve estimated using equation 1. (c) H_2O mixing ratio residuals after the subtraction of the solar term and the regression constant C_{01} from water vapor measurements (see text).

One can clearly see that the 2020 water vapor maximum is still present after the subtraction of solar impact, which was in any case minimal. It means that the 24th solar minimum was not responsible for the observed water vapor maximum in the 2020 summer. There should be another

https://doi.org/10.5194/angeo-2021-28
Preprint. Discussion started: 10 June 2021

Annales Geophysicae Discussions Open Access EGU

source of the 2020 water vapor maximum observed at middle latitudes in the upper mesosphere, which is discussed in the next section.

4.4. Results on the relationship between volcanic activity and the water vapor concentration maximum in 2020

Water vapor is one of the major volcanic gases and one might expect a potential influence of volcanic activity on the humidity level at the mesopause region via intrusions of volcanic water vapor into the stratosphere and their successive transport to the mesopause region by means of a general meridional atmospheric circulation. Unfortunately, there are no reliable estimations of the amount of volcanic water vapor injected into the atmosphere so far. Fortunately, there are satellite measurements of sulfur dioxide (SO_2), being a major volcanic gas as well. Below we consider SO_2 volcanic emissions injected into the atmosphere as a proxy for volcanic activity related to the present study.

We have used quantitative information on global volcanic activity represented by a long-term database of the volcanic SO_2 emission derived from ultraviolet satellite measurements from 1978 to 2019. The data (version 3) represent best estimates of the volcanic contribution to global atmospheric SO_2 concentrations (Carn et al., 2015; Carn, 2019) and can be downloaded from GES DISC Dataset: https://disc.gsfc.nasa.gov/datasets/MSVOLSO2L4_3/summary.

This database contains information on SO_2 plume altitudes varying from 2 to 28 km. Since several tens of volcanic eruptions occur each year, we have selected volcanic eruptions having SO_2 plume altitudes greater than 10 km in order to facilitate intrusions of SO_2 emissions (and probably volcanic water vapor) directly into the stratosphere in order to overcome a well-known freeze-drying water vapor effect at the tropopause region (Pinto et al., 1989; Brasseur and Solomon, 1986; Siebert et al., 2010). Then selected SO_2 plume altitudes (higher 10 km) have been averaged for each year to produce annual mean volcanic eruption altitudes. The result of these calculations is illustrated in Fig. 10, in which we can see the mean altitude maximum in 1991 due to the great Pinatubo eruption. Also, there is a secondary maximum in the volcanic activity recently happened in 2015 due to powerful high altitude volcanic eruptions that occurred in Italy, Chile, Ecuador, Papua New Guinea and Kamchatka. Below we concentrate on the analysis of recent volcanic activity from 2000 to 2019, which is related to the analyzed water vapor measurements for 2005–2020.

https://doi.org/10.5194/angeo-2021-28
Preprint. Discussion started: 10 June 2021

Annales Geophysicae
Discussions
Open Access

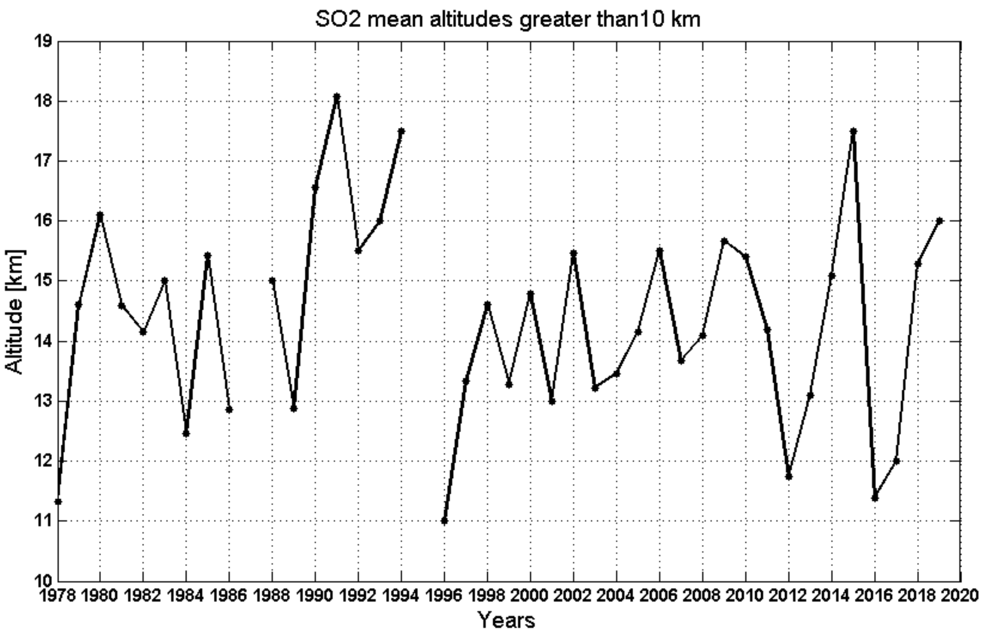

Figure 10. Time series of volcanic activity for 1978-2019, represented by annual mean SO_2 plume eruption altitudes per each year. Volcanic eruptions having SO_2 plume altitudes greater than 10 km have been selected for the analysis (see text).

We apply the MRA technique again as described above for solar activity, and now we add a volcanic activity term H_{SO2}:

$$H2O = C_{02} + C_{12} \cdot (t - 2005) + C_{22} \cdot F_{Lya}(t - t_{lag1}) + C_{32} \cdot H_{SO2}(t - t_{lag2}) \qquad (2)$$

H_{SO2} is the annual mean observed SO_2 plume altitude, C_{32} is the regression coefficient for volcanic activity (H_2O/ km), $H2O$ is the summer mean water vapour mixing ratio per each year, F_{Lya} is the Lyman α flux averaged over each summer season (June-July), t is the time, C_{02} is the regression constant; C_{12} is the regression coefficients characterizing the linear long-term trend (H2O/yr), C_{22} is the regression coefficient for solar activity, t_{lag1} is the phase time lag between water vapor and solar activity, t_{lag2} is the phase time lag between water vapor data and volcanic activity. We choose a fixed time lag equal to zero years for the solar activity term since there is no dependence between water vapor amount and solar activity at the mesopause as found in the previous section. The t_{lag2} value for the C_{32} coefficient is a variable parameter from 0 to 7 years since it is a completely unknown quantity between the mesopause water vapor and volcanic activity so far.

Figure 11 demonstrates the relationship between water vapour and SO_2 volcanic activity for 2005–2020. Figure 11a shows a moderate cross-correlation coefficient as a function of time lag,

https://doi.org/10.5194/angeo-2021-28
Preprint. Discussion started: 10 June 2021

Annales Geophysicae Discussions

having a maximum of +0.53 at the lag of 5 years (the black line). This correlation coefficient is significantly greater (by absolute value) than the cross-correlation coefficient between H_2O and solar activity (0÷ –0.2) found in the previous section. The red line illustrates the cross-correlation coefficient after shifting volcanic data by 5 years back in time, having now maximum at zero years.

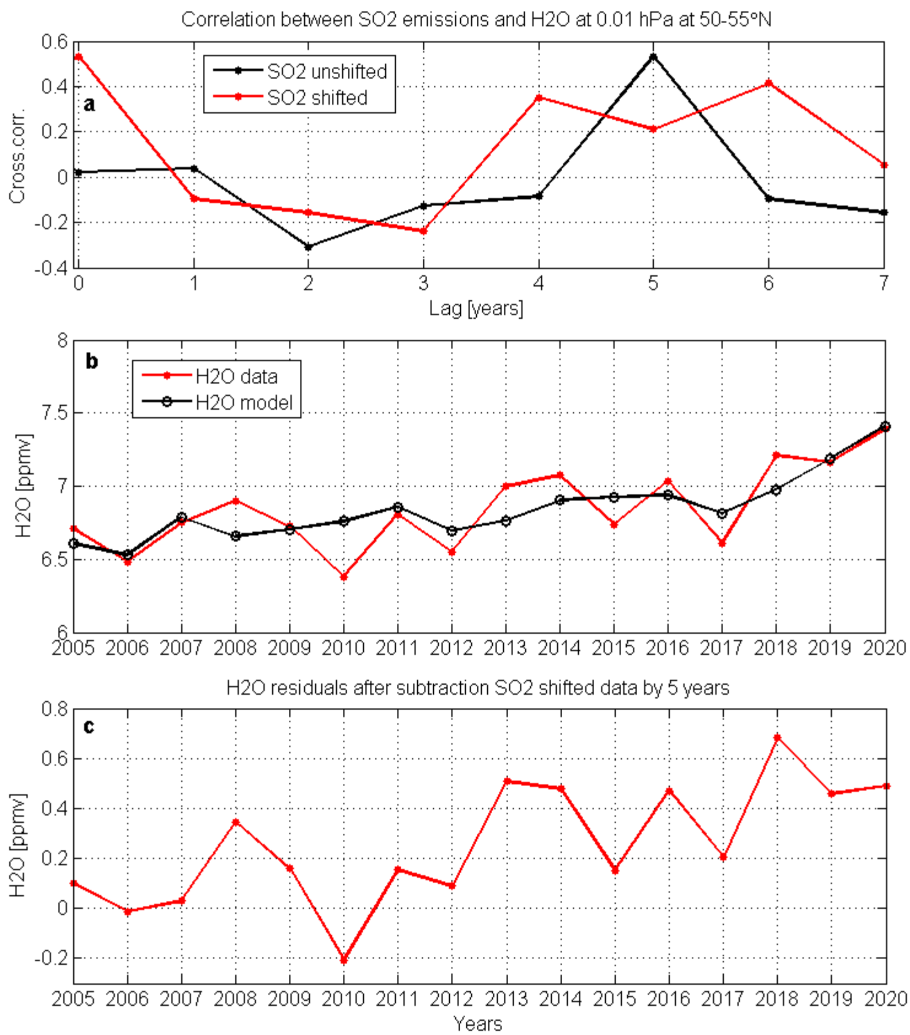

Figure 11. Relation between Aura/MLS water vapor (at 0.01 hPa at 50-55°N) and SO_2 plume emission altitude. (a) The black line shows a cross-correlation coefficient between water vapour and SO_2 altitude as a function of time lag in years. The red line illustrates the cross-correlation coefficient after shifting the volcanic SO_2 data by 5 years back in time. (b) The red line is the maximum value of H_2O mixing ratio of a Gaussian fit estimated at the middle latitudes 50-55°N at

https://doi.org/10.5194/angeo-2021-28
Preprint. Discussion started: 10 June 2021

0.01 hPa (see the red line in Fig. 6d) as well as the model regression curve (the black line) using equation 2, with the volcanic data being shifted by 5 years back. (c) H_2O mixing ratio residuals after the subtraction of the SO_2 volcanic term, shifted by 5 years back in time, the solar term $C_{22} \cdot F_{Lya}(t - t_{lag1})$ and the regression constant C_{02} from water vapor measurements (see equation 2).

We use the found time lag of 5 years in further analysis and in the Discussion. Figure 11b demonstrates the maximum H_2O mixing ratio value of a Gaussian fit estimated at the middle latitudes 50-55°N at 0.01 hPa (see the red line in Fig. 6d) as well as the model regression curve (the black line) using equation 2, with volcanic data being shifted by 5 years back. One can clearly see that now there is a perfect match between the model estimation and actual water vapour measurements in 2019 and 2020. After the subtraction of the $C_{32} \cdot H_{SO2}$ volcanic term from water vapor measurements, the solar term $C_{22} \cdot F_{Lya}(t - t_{lag1})$ and regression constant C_{02}, H_2O mixing ratio residuals are shown in Fig. 11c, demonstrating that there is no water vapor maximum in 2020 anymore. This confirms that high volcanic activity occurring in 2015 was one of the major sources of the observed water vapor maximum in the 2020 summer mesopause, those physical mechanisms being addressed below in the Discussion. At the same time, these two water vapour residual points (2019 and 2020) are not equal to zero since there is a clear positive trend in the amount of water vapor since 2010, which is explained by neither SO_2 volcanic data nor solar activity. There should be another atmospheric process responsible for the observed positive trend in water vapor at the summer mesopause, which might be related to the increase in methane concentration, leading to increasing H_2O in the middle atmosphere (Thomas and Olivero, 2001). The exact reason for the observed positive trend in the H_2O concentration is beyond the scope of the present paper.

5. Discussion

Noctilucent clouds observed at mid-latitudes are supposed to be more sensitive to any temperature and water vapor changes than NLCs at high latitudes since there are no highly saturated conditions at the summer mesopause at middle latitudes, i.e., when temperature is not far below the frost point (Russell III et al., 2014). It is poorly understood what processes are responsible for such icy patches at mid-latitudes at the summer mesopause. Occasional NLC observations at mid-latitudes can have different and even contradictory atmospheric mechanisms discussed in the literature. Indeed, Hultgren et al. (2011) have found that NLC enhancements observed in July 2009 were caused mainly by "*a combination of local temperature variations by*

https://doi.org/10.5194/angeo-2021-28
Preprint. Discussion started: 10 June 2021

diurnal tides, favorably located large-scale planetary waves, and general mesospheric temperature conditions below the average compared to previous years. The transport of NLC particles from higher latitudes has also been investigated but does not seem to be probable because of the short life-time of the visible clouds and hence the short distance traveled during the time period of existence". However, Nielsen et al. (2011), investigating the same NLC increase in July 2009, have demonstrated that "*These clouds occur due to a combination of advection from higher and colder latitudes, and in situ wave growth. The 5-day wave was the most dominant driver behind these clouds*". Herron et al. (2007) have come to the conclusion that the middle latitude NLC display observed above Logan, Utah (41.7°N) on 22 June 1995, was produced by the combined effect of a gravity wave (ether orographic or convective source) and the diurnal tide to give rise to low enough temperatures to form the observed NLC event. Gerding et al. (2013b) have concluded that NLC occurrence above Kühlungsborn (54°N) is most likely related to temperature variation by planetary waves and is less influenced by tidal temperature disturbances. Thus, the 2020 middle latitude NLC displays might be locally formed as well as being advected from higher to middle latitudes due to a great variety of atmospheric waves (gravity, planetary waves and tides), with a combination of the decreased temperature and the increased water vapor concentration at the bottom of the mesopause region.

Figures 4 and 5 demonstrate a slight drop in temperature at latitude bands of 45-50°N and 50-55°N at altitudes of 0.0215, 0.01 and 0046 hPa. The gradual temperature lessening started in 2016/2017 and lasted until 2020, with relative temperature decrease varying between 1.8% and 2.5%, depending on latitude band, altitude and various temperature statistics considered. However, water vapor has demonstrated a significantly greater relative increase of 12-15% in 2020 compared to 2017, when water vapor levels have started to increase (one can consider water vapor concentration equal to a mean value in 2017 over the period of 2005–2017). At first glance, the recent water vapor growth and its maximum in 2020 might be a primary source of the observed increase in NLC activity at middle latitudes in 2020. At the same time, the existence of ice particles at the summer mesopause is possible when air is supersaturated, i.e. the saturation ratio S (ratio of the water vapor local partial pressure to the saturated pressure of water vapor over a plain ice surface at a given temperature) is greater than 1. The saturation ratio is linearly proportional to the water vapor volume mixing ratio and proportional to the exponential function of inverse temperature, T, $[S \propto H2O \cdot \exp(6077.4/T)]$, meaning that S is a strong inverse function of low mesopause temperatures at 130–180 K (Gadsden and Schröder, 1989; Berger and von Zahn, 2002). We can demonstrate this effect by using actual values of water vapor and temperature measurements being analyzed. For example, if we take a water vapor increase from

https://doi.org/10.5194/angeo-2021-28
Preprint. Discussion started: 10 June 2021

Annales Geophysicae
Discussions

6.5 to 7.5 ppmv (see the red line in Fig. 11b) between 2017 and 2020, this H_2O increase results in the enhancement of the *S* value of 1.15 times. However, if we consider a temperature drop from 179 to 175 K between 2016 and 2020 (see the red line in Fig. 4a), then the *S* value increases of 2.17 times. Thus, from the point of view of the ice particle existence at the summer mesopause the observed temperature drop plays a more important role compared to the observed water vapor increase. At the same time, it is important to note that both the temperature drop and water vapor increase, occurred in the summer of 2020, have led to the increased saturation ratio, compared to the previous years, and hence to the pronounced increase of NLC activity as observed at middle latitudes in 2020.

At higher latitudes 55-60°N, NLC activity has demonstrated a different behavior from site to site. In particular, a maximum in NLC number (42 cases) has been observed in Lithuania (54-55°N) in the past 30 years, whereas NLC activity has demonstrated no maximum as seen from the Moscow region (55-56°N) in the past 60 years, taking into account tropospheric weather conditions. This result can be explained by the fact that the temperature drops as well as water vapor increases at higher latitudes (55-60°N) were not as strong as ones at lower latitudes, meaning that the saturation ratio was of about the same level as one in previous years at higher latitudes. That is why, at some sites the wave activity could play important role in increasing the saturation ratio (lower temperature and more humidity brought from higher latitudes) but at other site it was not like this.

The annual mean of SO_2 plume altitude in 2015 (for volcanic eruptions greater than 10 km altitude) have produced a positive impact on the maximum amount of water vapor at the summer mesopause in 2020, with the time lag of 5 years. This positive volcanic impact on the mesopause humidity is connected to the transport of water vapour from the lower stratosphere to the upper mesosphere and can be explained as follows. In the equatorial troposphere, there is an overturning wind circulation called the Hadley Cells, in which the warm air rising at the equator sinks at around 30°S and 30°N latitudes where the Hadley Cells end (Brasseur and Solomon, 1986). However, the Hadley Cells are not completely closed circulations. Part of the air penetrates into the stratosphere in the tropics, then traveling towards polar latitudes of the summer hemisphere, where it again rises to the summer mesosphere, and finally reaches the summer mesopause (Garcia and Solomon, 1983; Brasseur and Solomon, 1986). This meridional-vertical air circulation is supposed to be one of the main sources of water vapor at the mesopause region to form NLC ice particles (Thomas, 1991).

The 5-year phase lag found between the maximum in volcanic activity and the maximum in the water vapor amount at the mesopause at middle latitudes is supported by experimental studies

https://doi.org/10.5194/angeo-2021-28
Preprint. Discussion started: 10 June 2021

dealing with the transport time of minor atmospheric species from the troposphere to the stratosphere and mesosphere. The transport time of inert trace gases (N_2O, CF2C12, CFC13 and CC14) from the ground to the stratosphere (at 20-30 km altitude) have been observed to be of the order of 3-4 years (Stordal et al., 1985). Russell III et al. (1996) have found that the transport time of hydrogen fluoride (HF) trace gas is 5.9±2 years to be lifted from the lower troposphere to the mesosphere at 55 km altitude. The transport time of the CO_2 trace gas (as measured in a balloon-borne experiment) was found to be about 5 years to reach the polar stratosphere at 35 km altitude from the troposphere through the tropical upwelling (Bischof et al., 1985). Thus, it takes about 4–6 years for inert trace gases to reach the polar atmosphere at 30-55 km altitude from the tropical troposphere. Then it takes them two more years to rise throughout the mesosphere and reaching the mesopause region at 85-87 km altitude where NLC ice particles start to form. The latter is supported by a well know fact that first undoubtedly detected NLCs were discovered in June 1885, i.e., about two years after the great explosive Krakatoa eruption occurred in August 1883. Note that the most likely altitude of the Krakatoa eruption column was about 40–50 km (Self and Rampino, 1981; Carey and Sparks, 1986). As a result, the total time required for transporting volcanic water vapor from the tropical troposphere to the middle and polar mesopause is about 6-8 years. However, in the present analysis we have selected powerful volcanic eruptions having altitudes of more than 10 km to overcome the cold tropopause region and well-known freeze-drying effect for water vapor (Brasseur and Solomon, 1986; Pinto et al., 1989). Thus, the transport time of volcanic water vapor from the lower stratosphere to the polar and midlatitude mesopause is expected to be slightly less than 6-8 years, and the found time lag of 5 years matches well this estimation of water vapor time transport due to the general meridional-vertical air circulation. Note that a maximum in the NLC occurrence number and brightness was evident in 1995 following the powerful Pinatubo eruption in 1991 (Gadsden, 1998; Thomas and Olivero, 2001; Romejko et al., 2003), i.e., the NLC maximum occurred 4 years after the great volcanic eruption in 1991. This time shift corresponds to our result of a 5-year time delay, taking into account the fact that the great Pinatubo eruption produced a high volcanic plume reaching 25 km altitude (Considine et al., 2001; Carn et al., 2015), thus allowing volcanic water vapor to deeply penetrate into the upper stratosphere, with successive slow upward motion into the midlatitude mesopause region. Also, we emphasize that volcanic eruptions warm up the cold tropopause region that in turn facilitate a transfer of H_2O into the stratosphere across the tropopause (Considine et al., 2001).

https://doi.org/10.5194/angeo-2021-28
Preprint. Discussion started: 10 June 2021

Annales Geophysicae Discussions

6. Conclusions

The 2020 summer season has revealed frequent and widespread occurrences of noctilucent clouds in the Northern Hemisphere at middle latitudes between 45° and 55°N. In order to investigate a reason for this extraordinary NLC season, we have considered long-term Aura/MLS satellite data for all available summer periods from 2005 to 2020 so far. Both temperature and water vapor in the upper mesosphere and the mesopause region (between 75 and 90 km altitude) have been considered. Also, we have also analyzed solar and volcanic activity in search of possible reasons for the increased amount of water vapor and can conclude the following:

1. A moderate decrease (without any dramatic changes) in temperature has been observed beneath and at the middle latitude summer mesopause for the past years (2016–2020).
2. Water vapor concentration has significantly increased (by about 12-15%) in the 2020 summer compared to 2017, meaning that the summer mesopause at middle latitudes has become more wet. A combination of lower mesopause temperature and water vapor maximum at middle latitudes is the main reason for frequent and widespread occurrences of noctilucent clouds seen around the globe at middle latitudes in the 2020 summer.
3. The 24th solar cycle minimum cannot explain the strong increase in water vapor (and the H_2O maximum in 2020) for the past years since the correlation between Lyman-α flux and water vapor amount is very low (0÷ –0.2).
4. The increase in volcanic activity from 2013 to 2015 (and its maximum in 2015) explains the increased amount of water vapor in the upper mesosphere for the recent years (2018–2020) and its maximum in 2020 due to volcanic water vapor being injected into the stratosphere and transported into the upper mesosphere. The 5-year delay between volcanic activity and water vapor maximum is well explained by the general meridional-vertical atmospheric circulation.
5. Since volcanic activity has significantly decreased after 2015, we might expect a decrease in the amount of H_2O at the mesopause region and in NLC activity at middle latitudes that makes such NLC observations of great importance in the years to come.
6. Neither solar nor volcanic activity can explain a positive trend in water vapor in the upper mesosphere since 2010. There exists another atmospheric process responsible for the observed positive increase in water vapor at the bottom of the summer mesopause at middle latitudes.

Acknowledgements

The authors are grateful to all observers for their help in observing noctilucent clouds conducted in Japan, Canada, USA, Europe and Russia. The NLC photograph taken from Hokkaido has been provided by a staff of Nayoro astronomy observatory, Mr. Fumitake Watanabe. This work was

https://doi.org/10.5194/angeo-2021-28
Preprint. Discussion started: 10 June 2021

Annales Geophysicae Discussions

supported in part by the Japan Society for the Promotion of Science (JSPS) KAKENHI (Grant No. JP19H01956), by Meiji University (Grant No. MU-RMG 2019-21), by the Russian Foundation for Basic Research (Grant No. 19-05-00358a) and by the Science Committee of the Ministry of Education and Science of the Republic of Kazakhstan (Grant No. APO8856096). We thank the Aura/MLS team for providing high-quality temperature and water vapor data.

References

Berger, U., and von Zahn, U.: Icy particles in the summer mesopause region: three-dimensional modeling of their environment and two-dimensional modeling of their transport, J. Geophys. Res., 107, A11, 1366, doi:10.1029/2001JA000316, 2002.

Bischof, W., Borchers, R., Fabian, P., and Krüger, B.C.: Increased concentration and vertical distribution of carbon dioxide in the stratosphere, Nature, 316, 708-710, 1985.

Brasseur, G., and Solomon, S.: Aeronomy of the middle atmosphere. Second Edition, D. Reidel Publishing Company, Dordrecht, Holland, 1986.

Carey, S.N., and Sparks, R.S.J.: Quantitative models of fallout and dispersal of tephra from volcanic eruption columns, Bulletin of Volcanology, 48, 109–125, 1986.

Carn, S.: Multi-satellite volcanic sulfur dioxide L4 long-term global database V3, Greenbelt, MD, USA, Goddard Earth Science Data and Information Services Center (GES DISC), Accessed: Data Access 2020-11-11, 10.5067/MEASURES/SO2/DATA404, 2019.

Carn, S.A., Yang, K., Prata, A.J., and Krotkov, N.A.: Extending the long-term record of volcanic SO2 emissions with the Ozone Mapping and Profiler Suite (OMPS) Nadir Mapper, Geophys. Res. Lett., 42, 925-932, doi:10.1002/2014GL062437, 2015.

Considine, D.B., Rosenfield, J.E., and Fleming, E.L.: An interactive model study of the influence of the Mount Pinatubo aerosol on stratospheric methane and water trends, J. Geophys. Res., 106, D21, 27711-27727, 2001.

Dalin, P., Pertsev, N., Zadorozhny, A., Connors, M., Schofield, I., Shelton, I., Zalcik, M., McEwan, T., McEachran, I., Frandsen, S., Hansen, O., Andersen, H., Sukhodoev, V., Perminov, V., and Romejko, V.: Ground-based observations of noctilucent clouds with a northern hemisphere network of automatic digital cameras, J. Atmos. Sol.-Terr. Phys., 70, 1460-1472, doi:10.1016/j.jastp.2008.04.018, 2008.

Dalin, P., Perminov, V., Pertsev, N., and Romejko, V.: Updated long-term trends in mesopause temperature, airglow emissions, and noctilucent clouds, J. Geophys. Res., 125, e2019JD030814. https://doi.org/10.1029/2019JD030814, 2020.

https://doi.org/10.5194/angeo-2021-28
Preprint. Discussion started: 10 June 2021

DeLand, M.T., and Thomas, G.E.: Extending the SBUV PMC data record with OMPS NP, Atmos. Chem. Phys., 19, 11, 7913-7925, 2019.

Donahue, T.M., Guenther, B., and Blamont, J.E.: Noctilucent clouds in daytime: circumpolar particulate layers near the summer mesopause, J. Atm. Sci., 29, 1205-1209, 1972.

Dubietis, A., Dalin, P., Balčiunas, R., and Černis, K.: Observations of noctilucent clouds from Lithuania, J. Atm. Sol.-Terr. Phys., 72, 14-15, 1090-1099, 2010.

Dubietis, A., Dalin, P., Balčiunas, R., Černis, K., Pertsev, N., Sukhodoev, V., Perminov, V., Zalcik, M., Zadorozhny, A., Connors, M., Schofield, I., McEwan, T., McEachran, I., Frandsen, S., Hansen, O., Andersen, H., Grønne, J., Melnikov, D., Manevich, A., and Romejko, V.: Noctilucent clouds: modern ground-based photographic observations by a digital camera network, Applied Optics, 50, 28, F72-F79, doi:10.1364/AO.50.000F72, 2011.

Froidevaux, L., Livesey, N.J., Read, W.G., Jiang, Y.B., Jiménez, C.C., Filipiak, M.J., Schwartz, M.J., Santee, M.L., Pumphrey, H.C., Jiang, J.H., Wu, D.L., Manney, G.L., Drouin, B.J., Waters, J.W., Fetzer, E.J., Bernath, P.F., Boone, C.D., Walker, K.A., Jucks, K.W., Toon, G.C., Margitan, J.J., Sen, B., Webster, C.R., Christensen, L.E., Elkins, J.W., Atlas, E., Lueb, R.A., and Hendershot, R.: Early validation analyses of atmospheric profiles from EOS MLS on the Aura satellite, IEEE Transactions on Geoscience and Remote Sensing, 44, 5, 1106-1121, 2006.

Gadsden, M., and Schröder, W.: Noctilucent Clouds, Springer, New York, 165 pp, 1989.

Gadsden, M.: The North-West Europe data on noctilucent clouds: a survey, J. Atmos. Terr. Phys., 60, 1163-1174, 1998.

Garcia, R.R., and Solomon, S.: A numerical model of the zonally averaged dynamical and chemical structure of the middle atmosphere, J. Geophys. Res., 88, C2, 1379-1400, 1983.

Gerding, M., Höffner, J., Hoffmann, P., Kopp, M., and Lübken, F.-J.: Noctilucent cloud variability and mean parameters from 15 years of lidar observations at amid-latitude site (54°N, 12°E), J. Geophys. Res. Atmos., 118, 317–328, doi:10.1029/2012JD018319, 2013a.

Gerding, M., Kopp, M., Hoffmann, P., Höffner, J., and Lübken, F.-J.: Diurnal variations of midlatitude NLC parameters observed by daylight-capable lidar, and their relation to ambient parameters, Geophys. Res. Lett., 40, 6390–6394, doi:10.1002/2013GL057955, 2013b.

Herron, J.P., Wickwar, V.B., Espy, P.J., and Meriwether, J.W.: Observations of a noctilucent cloud above Logan, Utah (41.7°N, 111.8°W) in 1995, J. Geophys. Res., 112, D19203, doi:10.1029/2006JD007158, 2007.

Hultgren, K., Körnich, H., Gumbel, J., Gerding, M., Hoffmann, P., Lossow, S., and Megner, L.: What caused the exceptional mid-latitudinal noctilucent cloud event in July 2009?, J. Atmos. Sol.-Terr. Phys., 73, 14-15, 2125-2131, 2011.

https://doi.org/10.5194/angeo-2021-28
Preprint. Discussion started: 10 June 2021

Annales Geophysicae Discussions

Kirkwood, S., Dalin, P., and Réchou, A.: Noctilucent clouds observed from the UK and Denmark – trends and variations over 43 years, Ann. Geophys., 26, 1243-1254, 2008.

Lambert, A., Read, W.G., Livesey, N.J., Santee, M. L., Manney, G.L., Froidevaux, L., Wu, D.L., Schwartz, M.J., Pumphrey, H.C., Jimenez, C., Nedoluha, G.E., Cofield, R.E., Cuddy, D.T., Daffer, W.H., Drouin, B.J., Fuller, R.A., Jarnot, R.F., Knosp, B.W., Pickett, H.M., Perun, V.S., Snyder, W.V., Stek, P.C., Thurstans, R.P., Wagner, P.A., Waters, J.W., Jucks, K.W., Toon, G.C., Stachnik, R.A., Bernath, P.F., Boone, C.D., Walker, K.A., Urban, J., Murtagh, D., Elkins, J.W., and Atlas, E.: Validation of the Aura Microwave Limb Sounder middle atmosphere water vapor and nitrous oxide measurements, J. Geophys. Res., 112, D24S36, 2007.

Nielsen, K., Nedoluha, G.E., Chandran, A., Chang, L.C., Barker-Tvedtnes, J., Taylor, M.J., Mitchell, N.J., Lambert, A., Schwartz, M.J., and Russell III, J.M.: On the origin of mid-latitude mesospheric clouds: the July 2009 cloud outbreak, J. Atmos. Sol.-Terr. Phys., 73, 14-15, 2118-2124, 2011.

Pertsev, N., Dalin, P., Perminov, V., Romejko, V., Dubietis, A., Balčiunas, R., Černis, K., and Zalcik, M.: Noctilucent clouds observed from the ground: sensitivity to mesospheric parameters and long-term time series, Earth Planets Space, 66, 98, doi:10.1186/1880-5981-66-98, 2014.

Pinto, J.P., Turco, R.P., and Toon, O.B.: Self-limiting physical and chemical effects in volcanic eruption clouds, J. Geophys. Res., 94, D8, 11165-11174, 1989.

Read, W.G., Lambert, A., Bacmeister, J., Cofield, R.E., Christensen, L.E., Cuddy, D.T., Daffer, W.H., Drouin, B.J., Fetzer, E., Froidevaux, L., Fuller, R., Herman, R., Jarnot, R.F., Jiang, J.H., Jiang, Y.B., Kelly, K., Knosp, B.W., Kovalenko, L.J., Livesey, N.J., Liu, H.-C., Manney, G.L., Pickett, H.M., Pumphrey, H.C., Rosenlof, K.H., Sabounchi, X., Santee, M.L., Schwartz, M.J., Snyder, W.V., Stek, P.C., Su, H., Takacs, L.L., Thurstans, R.P., Vömel, H., Wagner, P.A., Waters, J.W., Webster, C.R., Weinstock, E.M., and Wu, D.L.: Aura Microwave Limb Sounder upper tropospheric and lower stratospheric H2O and relative humidity with respect to ice validation, J. Geophys. Res., 112, D24S35, 2007.

Romejko, V.A., Dalin, P.A., and Pertsev, N.N.: Forty years of noctilucent cloud observations near Moscow: database and simple statistics, J. Geophys. Res., 108, D8, 8443, doi:10.1029/2002JD002364, 2003.

Russell III, J.M., Luo, M., Cicerone, R.J., and Deaver, L.E.: Satellite confirmation of the dominance of chlorofluorocarbons in the global stratospheric chlorine budget, Nature, 379, 526–529, 1996.

https://doi.org/10.5194/angeo-2021-28
Preprint. Discussion started: 10 June 2021

Annales Geophysicae Discussions

Russell III, J.M., Rong, P., Hervig, M.E., Siskind, D.E., Stevens, M.H., Bailey, S.M., and Gumbel, J.: Analysis of northern midlatitude noctilucent cloud occurrences using satellite data and modeling, J. Geophys. Res. Atmos., 119, 3238-3250, doi:10.1002/2013JD021017, 2014.

Russell III, J.M., Bailey, S.M., Gordley, L.L., Rusch, D.W., Horányi, M., Hervig, M.E., Thomas, G.E., Randall, C.E., Siskind, D.E., Stevens, M.H., Summers, M.E., Taylor, M.I., Englert, C.R., Espy, P.J., McClintock, W.E., and Merkel, A.W.: Aeronomy of Ice in the Mesosphere (AIM) Mission: overview and early science results, J. Atmos. Sol.-Terr. Phys., 71, 289–299, 2009.

Schwartz, M.J., Lambert, A., Manney, G.L., Read, W.G., Livesey, N.J., Froidevaux, L., Ao, C.O., Bernath, P.F., Boone, C.D., Cofield, R.E., Daffer, W.H., Drouin, B.J., Fetzer, E.J., Fuller, R.A., Jarnot, R.F., Jiang, J.H., Jiang, Y.B., Knosp, B.W., Krüger, K., Li, J.-L. F., Mlynczak, M.G., Pawson, S., Russell III, J.M., Santee, M.L., Snyder, W.V., Stek, P.C., Thurstans, R.P., Tompkins, A.M., Wagner, P.A., Walker, K.A., Waters, J.W., and Wu, D.L.: Validation of the Aura Microwave Limb Sounder temperature and geopotential height measurements, J. Geophys. Res., 113, D15S11, 2008.

Self, S., and Rampino, M.: The 1883 eruption of Krakatau. Nature, 294, 699–704, 1981.

Siebert, L., Simkin, T., and Kimberly, P.: Volcanoes of the World. Third Edition, University of California Press, Los Angeles, 2010.

Stevens, M.H., Lieberman, R.S., Siskind, D.E., McCormack, J.P., Hervig, M.E., and Englert, C.R.: Periodicities of polar mesospheric clouds inferred from a meteorological analysis and forecast system, J. Geophys. Res. Atmos., 122, 4508–4527, doi:10.1002/2016JD025349, 2017.

Stordal, F., Isaksen, I.S.A., and Horntveth, K.: A diabatic circulation two-dimensional model with photochemistry: simulations of ozone and long-lived tracers with surface sources, J. Geophys. Res., 90, D3, 5757-5776, 1985.

Suzuki, H., Sakanoi, K., Nishitani, N., Ogawa, T., Ejiri, M.K., Kubota, M., Kinoshita, T., Murayama, Y., and Fujiyoshi, Y.: First imaging and identification of a noctilucent cloud from multiple sites in Hokkaido (43.2–44.4°N), Japan, Earth Planets Space, 68, 182, doi:10.1186/s40623-016-0562-6, 2016.

Taylor, M.J., Gadsden, M., Lowe, R.P., Zalcik, M.S., and Brausch, J.: Mesospheric cloud observations at unusually low latitudes, J. Atmos. Sol.-Terr. Phys., 64, 8, 991–999, 2002.

Thomas, G.E.: Solar Mesosphere Explorer measurements of polar mesospheric clouds (noctilucent clouds), J. Atmos. Terr. Phys., 46, 9, 819-824, 1984.

Thomas, G.E.: Mesospheric clouds and the physics of the mesopause region, Rev. Geophys., 29, 4, 553-575, 1991.

Thomas, G.E., and Olivero, J.: Noctilucent clouds as possible indicators of global change in the mesopause, Adv. Space Res., 28, 7, 937-946, 2001.

Waters, J.W., Froidevaux, L., Harwood, R.S., Jarnot, R.F., Pickett, H.M., Read, W.G., Siegel, P.H., Cofield, R.E., Filipiak, M.J., Flower, D.A., Holden, J.R., Lau, G.K., Livesey, N.J., Manney, G.L., Pumphrey, H.C., Santee, M.L., Wu, D.L., Cuddy, D.T., Lay, R.R., Loo, M.S., Perun, V.S., Schwartz, M.J., Stek, P.C., Thurstans, R.P., Boyles, M.A., Chandra, K.M., Chavez, M.C., Chen, G-S., Chudasama, B.V., Dodge, R., Fuller, R.A., Girard, M.A., Jiang, J.H., Jiang, Y., Knosp, B.W., LaBelle, R.C., Lam, J.C., Lee, K.A., Miller, D., Oswald, J.E., Patel, N.C., Pukala, D.M., Quintero, O., Scaff, D.M., Van Snyder, W., Tope, M.C., Wagner, P.A., and Walch, M.J.: The Earth Observing System Microwave Limb Sounder (EOS MLS) on the Aura satellite, IEEE Transactions on Geoscience and Remote Sensing, 44, 5, 1075-1092, 2006.

Wickwar, V.B., Taylor, M.J., Herron, J.P., and Martineau, B.A.: Visual and lidar observations of noctilucent clouds above Logan, Utah, at 41.7°N, J. Geophys. Res., 107, D7, 4054, doi:10.1029/2001JD001180, 2002.

https://doi.org/10.5194/angeo-2021-28
Preprint. Discussion started: 10 June 2021

Figure captions

Figure 1. An example of Aura/MLS data shown at the latitude band of 45-50°N at 0.0046 hPa (about 84 km) during the summer time between 25 May and 13 August 2009. (Upper panel) Zonal mean nighttime temperatures (the black line with dots), the red curve represents an inverse Gaussian fit to the data, the green dot shows the minimum of a Gaussian fit. (Lower panel) Zonal mean nighttime H_2O mixing ratio values (the black line with dots), the red curve shows a Gaussian fit to the data, the green dot marks the maximum of a Gaussian fit.

Figure 2. An example image of noctilucent clouds as seen from Hokkaido, Japan (44.3°N, 142.2°E) on the night of 17/18 July 2020. Comet NEOWISE is clearly seen in the image. The NLC photograph taken from Hokkaido has been provided by a staff of Nayoro astronomy observatory, Mr. Fumitake Watanabe.

Figure 3. The number of displays of noctilucent clouds as observed from latitudes below 50°N as a function of time. The black line with triangles shows NLC displays as observed in North America (Canada and USA observations), the blue line with open circles illustrates NLC sightings as observed from Russia, the red line with dots is NLC events as seen from Western Europe.

Figure 4. Aura/MLS temperature time series for summer periods of 2005–2020 at different latitude bands (45-50; 50-55; 55-60°N) and pressure levels of 0.0215 hPa (about 74 km) and 0.01 hPa (about 79 km). The black line indicates a minimum value of the zonal mean nighttime temperature for a summer season (between 25 May and 13 August), the red line is a minimum value of an inverse Gaussian fit, the blue line shows the mean of the zonal mean nighttime temperature for a summer period. Error bars indicate one standard deviation for each point.

Figure 5. Aura/MLS temperature time series for summer periods of 2005–2020 at different latitude bands (45-50; 50-55; 55-60°N) and pressure levels of 0.0046 and 0.0022 hPa. The black line indicates a minimum value of the zonal mean nighttime temperature for a summer season (between 25 May and 13 August), the red line is a minimum value of an inverse Gaussian fit, the blue line shows the mean of the zonal mean nighttime temperature for a summer period. Error bars indicate one standard deviation for each point.

Figure 6. Aura/MLS water vapor mixing ratio [ppmv] time series for summer periods of 2005–2020 at different latitude bands (45-50; 50-55; 55-60°N) and pressure levels of 0.0215 hPa (about

https://doi.org/10.5194/angeo-2021-28
Preprint. Discussion started: 10 June 2021

Annales Geophysicae
Discussions
Open Access

74 km) and 0.01 hPa (about 79 km). The black line indicates a maximum value of the nighttime H_2O zonal mean for a summer season between 25 May and 13 August, the red line is a maximum value of a Gaussian fit, the blue line shows the mean of the nighttime H_2O zonal mean for a summer period. Error bars indicate one standard deviation for each point.

Figure 7. Aura/MLS water vapor mixing ratio [ppmv] time series for summer periods of 2005–2020 at different latitude bands (45-50; 50-55; 55-60°N) and pressure levels of 0.0046 hPa (about 84 km) and 0.0022 hPa (about 89 km). The black line indicates a maximum value of the nighttime H_2O zonal mean for a summer season between 25 May and 13 August, the red line is a maximum value of a Gaussian fit, the blue line shows the mean of the nighttime H_2O zonal mean for a summer period. Error bars indicate one standard deviation for each point.

Figure 8. Summer mean values of solar Lyman-α flux for the period of 1947–2020.

Figure 9. Relationship between water vapor and solar activity for 2005–2020. Solar activity is represented by Lyman-α flux measurements. (a) cross-correlation coefficient as a function of time lag. (b) the red line shows the maximum value of H_2O mixing ratio of a Gaussian fit estimated at middle latitudes 50-55°N at 0.01 hPa (the red line in Fig. 6d), the black line is the model regression curve estimated using equation 1. (c) H_2O mixing ratio residuals after the subtraction of the solar term and the regression constant C_{01} from water vapor measurements (see text).

Figure 10. Time series of volcanic activity for 1978-2019, represented by annual mean SO_2 plume eruption altitudes per each year. Volcanic eruptions having SO_2 plume altitudes greater than 10 km have been selected for the analysis (see text).

Figure 11. Relation between Aura/MLS water vapor (at 0.01 hPa at 50-55°N) and SO_2 plume emission altitude. (a) The black line shows a cross-correlation coefficient between water vapour and SO_2 altitude as a function of time lag in years. The red line illustrates the cross-correlation coefficient after shifting the volcanic SO_2 data by 5 years back in time. (b) The red line is the maximum value of H_2O mixing ratio of a Gaussian fit estimated at the middle latitudes 50-55°N at 0.01 hPa (see the red line in Fig. 6d) as well as the model regression curve (the black line) using equation 2, with the volcanic data being shifted by 5 years back. (c) H_2O mixing ratio residuals after the subtraction of the SO_2 volcanic term, shifted by 5 years back in time, the solar term $C_{22} \cdot F_{Lya}(t - t_{lag1})$ and the regression constant C_{02} from water vapor measurements (see equation 2).